

# Iterative Learning–Based Nonlinear Model Predictive Control of an Underactuated Autonomous Surface Vessel in Current Fields

Hannes Homburger<sup>1</sup>, Katrin Baumgärtner<sup>2</sup>, Stefan Wirtensohn<sup>1</sup>, Moritz Diehl<sup>3</sup>, and Johannes Reuter<sup>1</sup>

**Abstract**—Efficient and safe autonomous control of surface vessels is seminal for the future of maritime transport systems. In this paper, we use an iterative learning–based nonlinear model predictive control scheme leveraging past experiences of the motion of vessels in a current field to reach optimal behavior. We define an optimal control problem including a detailed vessel model but only a roughly estimated current model. This current model is improved from trial to trial. The learned controller is compared to a linear track controller, a zero–offset nonlinear model predictive controller without current information, and a nonlinear model predictive controller including a perfect model of the current field. The results of this comparison show that by including experiences from previous trials, the controller can improve its performance significantly. We believe that numerical optimal control has the potential to disrupt the future control design of maritime systems.

## I. INTRODUCTION

Maritime transport systems have a significant impact on the global transport of goods and people. Nowadays, controlling ferries [1], [2] and water taxis [3], [4] make an important contribution to local public transport in many cities located close to water areas. Recently, different numerical optimal control methods have been employed to improve the efficiency and the safety of autonomous surface vessels (ASV) [5]–[7] especially in confined inland shipping scenarios [8]–[11]. These scenarios are characterized by the fact that vessels have to follow narrow sea routes, which exposes them to strongly varying currents on their way. These currents are a dominant but difficult–to–model part of the vessel’s dynamics that leads to model–plant mismatch [12]–[14]. However, the same routes are repeatedly traveled by ferries and water taxis. Human captains can use their experiences from previous runs in control of a vessel and employ them in planning its future behavior. This motivates the question of how to use previous experiences in automatic decisions and control. Recent contributions to iterative learning control (ILC) [15], [16] and nonlinear model predictive control (NMPC) [17] present methods to answer this question and reach optimal behavior. In this paper, we present an iterative learning–based NMPC approach to optimal tracking control of an underactuated ASV under the presence of currents. In contrast to general model learning approaches, the proposed approach learns only a model correction along

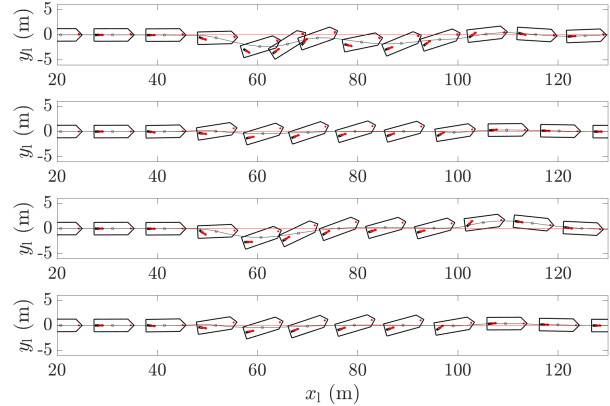


Fig. 1. Closed–loop trajectories using linear track control (top row), NMPC with perfect current model (second row), NMPC without current model (third row), and 5<sup>th</sup> trial of ILC NMPC (last row) in a benchmark scenario. The significant current is located in the area between  $50 \text{ m} \leq x_1 \leq 100 \text{ m}$ .

the optimal trajectory and therefore requires a small amount of experimental data. The behavior of different controllers in a benchmark scenario is shown in Figure 1. The paper is structured as follows: In Section II, the optimal control problem (OCP) is formulated including a presentation of the vessel dynamics in current fields. In Section III, the NMPC control problem and the disturbance estimation scheme are presented. This control scheme is extended to an iterative learning approach in Section IV. In Section V, the setup and results of numerical experiments are presented. Finally, Section V concludes the paper with a discussion and presents ideas for future work.

## II. OPTIMAL CONTROL PROBLEM FORMULATION

Following standard notation [17], we consider a finite horizon discrete time OCP including a fixed initial state

$$\underset{\substack{x_0, \dots, x_N, \\ u_0, \dots, u_{N-1}}}{\text{minimize}} \quad \sum_{k=0}^{N-1} L_k(x_k, u_k) + E(x_N) \quad (1a)$$

$$\text{subject to} \quad x_0 - \tilde{x}_0 = 0, \quad (1b)$$

$$x_{k+1} - F_k(x_k, u_k) = 0, \quad k = 0, \dots, N-1, \quad (1c)$$

$$h_k(x_k, u_k) \leq 0, \quad k = 0, \dots, N-1, \quad (1d)$$

where  $N \in \mathbb{N}$  denotes the number of discrete time steps,  $x_k \in \mathbb{R}^{n_x}$  with  $k = 0, \dots, N$  denotes the state trajectory,  $u_k \in \mathbb{R}^{n_u}$  with  $k = 0, \dots, N-1$  denotes the input trajectory,  $L_k : \mathbb{R}^{n_x} \times \mathbb{R}^{n_u} \rightarrow \mathbb{R}$  with  $k = 0, \dots, N-1$  denotes the stage costs,  $E : \mathbb{R}^{n_x} \rightarrow \mathbb{R}$  denotes the terminal cost,  $\tilde{x}_0 \in \mathbb{R}^{n_x}$  denote the fixed initial state, the discrete time system dynamics are denoted by  $F_k : \mathbb{R}^{n_x} \times \mathbb{R}^{n_u} \rightarrow \mathbb{R}^{n_x}$ , the path constraints

<sup>1</sup> Institute of System Dynamics, HTWG Konstanz – University of Applied Sciences, 78462 Konstanz, Germany  
 hhomburg@htwg-konstanz.de

<sup>2</sup> Department of Microsystems Engineering (IMTEK), University of Freiburg, 79110 Freiburg, Germany

<sup>3</sup> Department of Microsystems Engineering (IMTEK) and Department of Mathematics, University of Freiburg, 79110 Freiburg, Germany

are denoted by  $h_k : \mathbb{R}^{n_x} \times \mathbb{R}^{n_u} \rightarrow \mathbb{R}^{n_h}$  with  $k = 0, \dots, N-1$ , and  $n_x, n_u, n_h \in \mathbb{N}$  denote the state dimension, the control dimension, and the number of scalar inequality constraints. The discrete time OCP (1) is obtained from the discretization of a continuous time problem using direct multiple-shooting with a piecewise constant control parametrization [18]. The goal is to follow a predefined path with a vessel. The different parts of the corresponding OCP are presented in detail below.

### A. System Dynamics

In confined water scenarios, pitch, roll, and heave motion are neglected due to calm water conditions [19]. Based on these assumptions, a nonlinear three-degree-of-freedom (3-DOF) model of the following form is used

$$\dot{\eta} = J(\psi)v_r + \dot{\eta}_c(\eta), \quad (2a)$$

$$\dot{v}_r = M^{-1} [\tau_a^-(a^-, v_r) + \tau_d - M_{RB}\dot{v}_c - C_{RB}(v_r + v_c)(v_r + v_c) - N(v_r)v_r], \quad (2b)$$

where  $\eta = (x_1, y_1, \psi)^T \in \mathbb{R}^3$  denotes the vessel's pose in a local east-north-up (ENU) frame with position given by  $x_1$  and  $y_1$ , and  $\psi$  denotes the vessel's yaw angle referenced to the  $x_1$ -axis. Vector  $v_r = (u_r, v_r, r_r)^T$  denotes the body-fixed velocity relative to the flowing water with the relative velocity in the surge direction denoted by  $u_r$ , the relative velocity in the sway direction denoted by  $v_r$ , and the angular velocity of the yaw angle denoted by  $r_r$ ,  $J(\psi)$  denotes the rotation matrix dependent on  $\psi$ ,  $\dot{\eta}_c(\eta)$  denotes a position-dependent non-rotational current field,  $M = M_A + M_{RB}$  denotes the invertible mass matrix given by the sum of the added mass matrix denoted by  $M_A$  and the mass matrix of the rigid body denoted by  $M_{RB}$ , the Coriolis matrix is denoted by  $C_{RB}$ , the nonlinear hydrodynamic damping effects are modeled in  $N$ ,  $\tau_d$  denotes a generalized force vector of unmodeled internal and external effects, and  $v_c = J^{-1}(\psi)\dot{\eta}_c(\eta)$  models the current in the body-fixed frame with the corresponding total time derivative  $\dot{v}_c$ .

*Actuator configuration and different control modes:* The system input is given by the actuator state collected in  $a \in \mathbb{R}^{n_a}$ . The dynamics of the actuators are controlled by lower-level controllers and are neglected due to their fast dynamics compared to the dynamics of the vessel. In most cases, the actuator configuration is the only part of the considered vessel model (2) that differs qualitatively between different vessels and between different tasks. The actuator configuration is denoted by  $\tau_a : \mathbb{R}^{n_a} \times \mathbb{R}^3 \rightarrow \mathbb{A} \subseteq \mathbb{R}^3, a \times v_r \mapsto \tau_a$ , where the controlled force and torque vector is given by  $\tau_a = (X_a, Y_a, N_a)^T$  with the applied force in surge direction denoted by  $X_a$ ,  $Y_a$  denotes the applied force in sway direction, and the applied torque in yaw direction is denoted by  $N_a$ . During the operation of a ship, a distinction is made between different modes [1]: While in the *docking mode* all actuators are employed for precise dynamic positioning, to move between waypoints in the *transit mode* only a subset of the actuators is used. In the *transit mode*, often only the steering angle is varied while a constant thrust of the main propellers is used and bow

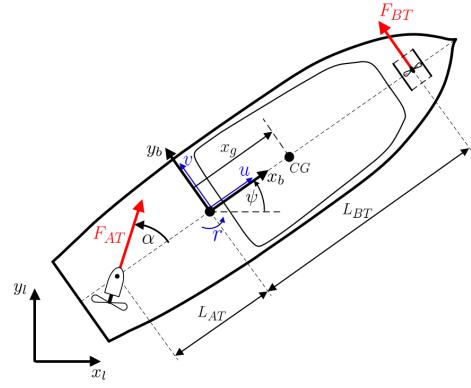


Fig. 2. Schematic drawing of the research vessel *Solgenia* including the relevant coordinate frames and the actuator configuration.

thrusters are deactivated. They are deactivated because they are generally inefficient at high surge speeds. The reduced actuator configuration of the transit mode is represented by  $\tau_a^- : \mathbb{R}^{n_a^-} \times \mathbb{R}^3 \rightarrow \mathbb{T} \subseteq \mathbb{A}, a^- \times v_r \mapsto \tau_a^-$ , where  $n_a^- \leq n_a$  is the number of active actuators in the *transit mode* and  $\mathbb{T}$  denotes the set containing the controlled force and torque vectors applicable in this configuration. In *transit mode*  $\tau_a^-$  is often restricted, thus control allocation cannot be applied [19] - the so-called underactuated case. The discrete time model used in (1c) is given by the discretization of the continuous time dynamics (2) with  $n_{\text{step}}$  steps of the explicit Runge-Kutta method of order four (RK4).

*Output equation and resulting state space model:* Surface vessels are usually equipped with a Global Positioning System (GPS) supplying discrete time measurements of the vessel's pose and the vessel's velocity in the ENU frame. These properties motivate the nonlinear state space model

$$x_{k+1} = F_k(x_k, u_k), \quad (3a)$$

$$y_k = H(x_k), \quad (3b)$$

where  $y_k \in \mathbb{R}^{n_y}$  denotes the measurement vector with dimension  $n_y = 6$  and  $H(x_k) = (\eta_k^T, \dot{\eta}_k^T)^T$  denotes the measurement equation. Note that the currents can not be measured adequately in most cases. In the literature, more information can be found about the dynamic model of a vessel [19], [20], the influence of current [12]–[14], and the different control modes of a vessel [1], [19]. Figure 2 depicts a visualization of the research vessel *Solgenia* used for this study.

### B. Tracking Cost Function

We consider a cost function (1a) as the sum of stage costs along the trajectory and the terminal cost term evaluated at the final state. To determine these parts of the cost function we define the goals to be reached in the transit mode:

- 1) Stay close to the predefined path.
- 2) Use the least possible control effort.

These goals are contradictory but common for tracking problems [15] and are combined in the cost function to

$$L_k(x_k, u_k) = l(e(x_k, u_k))\Delta T_k,$$

where  $e : \mathbb{R}^{n_x} \times \mathbb{R}^{n_u} \rightarrow \mathbb{R}^{n_e}$  denotes the tracking error,  $l : \mathbb{R}^{n_e} \rightarrow \mathbb{R}$  is a strictly convex function that penalizes the tracking error usually, but not necessarily, in quadratic form, and  $\Delta T_k > 0$  is the length of the  $k$ -th shooting interval. We assume that  $e$  and  $l$  are twice continuously differentiable functions and that  $l(z)$  has a global minimum at  $z = 0$  with value  $l(0) = 0$ . Therefore, the optimal behavior of the vessel is considered to be a trade-off between the described goals. The terminal cost function is determined as

$$E(x_N) = e(x_N, 0)^\top P e(x_N, 0), \quad (4)$$

where  $P$  is a positive definite matrix to approximate the infinite horizon costs.

### C. Initial and Path Constraints

The initial state  $\tilde{x}_0$  used in (1b) determines the state at the start of the optimal trajectory and is given by the current state of the vessel. With the path constraints (1d) hard inequality constraints along the predicted trajectories can be considered. In the transit scenario, there is only one path constraint: The actuator states should be limited. Therefore, (1d) can be formulated as

$$h_k(x_k, u_k) = \begin{pmatrix} \underline{u} - u_k \\ u_k - \bar{u} \end{pmatrix} \leq 0, \quad (5)$$

where each scalar inequality constraint is evaluated separately, the minimal input is denoted by  $\underline{u}$  and the maximal input is denoted by  $\bar{u}$ .

## III. CONTROLLER DESIGN AND STATE ESTIMATION

In this section the design of an NMPC scheme including a state and disturbance observer is described based on the presented discrete time OCP.

### A. State and Disturbance Estimation

The current  $\dot{\eta}_c(\eta)$  significantly influences the system dynamics (2). However, it is a formidable task to model the current map. This motivates us to split up the position-dependent current field with

$$\dot{\eta}_c(\eta) = \dot{\eta}_{c,M}(\eta, \theta) + d(\eta) \quad (6)$$

in two parts, where  $\dot{\eta}_{c,M}(\eta, \theta)$  denotes the modeled current map with parameter vector  $\theta \in \mathbb{R}^{n_\theta}$  that is fixed in non-adaptive control approaches and  $d : \mathbb{R}^3 \rightarrow \mathbb{R}^3$  denotes the position-dependent error of the modeled current map. Following a standard approach for disturbance estimation [17], we introduce the augmented model

$$\bar{x}_{k+1} = \begin{pmatrix} x_{k+1} \\ d_{k+1} \end{pmatrix} = \begin{pmatrix} F_M(x_k, u_k, d_k, \theta) \\ d_k \end{pmatrix} + w_k, \quad (7a)$$

$$y_k = H(x_k) + v_k, \quad (7b)$$

for the estimation task, where  $F_M(\cdot)$  denotes the system dynamics (3a) including the error current model (6),  $w_k \in \mathbb{R}^{n_x}$  denotes the stochastic disturbances and  $v_k \in \mathbb{R}^{n_y}$  denotes the measurement noise, each at the  $k$ -th time instance. With assumed probability density functions (PDF), the estimation

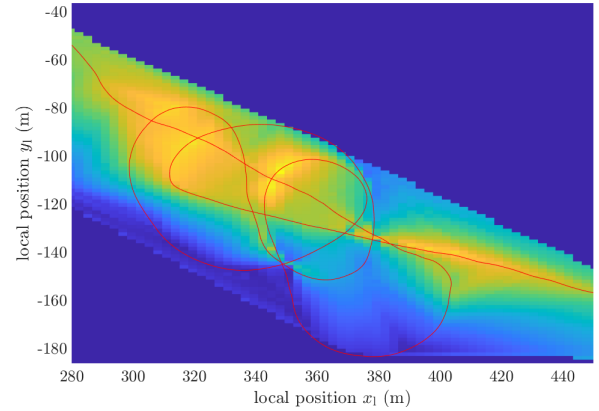


Fig. 3. Exemplary map of modeled current amplitudes on a river. The improvable generalization of the employed interpolation model motivates the usage of ILC. The used data is recorded in a full-scale experiment driving 600 s on the Rhine river in Konstanz [21]. The vessel's trajectory is plotted in red and starts from the right side. The interpolated current model has a range between 0 m/s (dark blue) and 1.2 m/s (bright yellow).

problem corresponding to (7) can be addressed using nonlinear data fusion algorithms e.g. Moving Horizon Estimation (MHE) or nonlinear Kalman Filter algorithms in case of unimodal distributions.

### B. Controller Design

To reach offset-free tracking in MPC schemes, two ideas are widespread [17]: Adding integral action or employing a disturbance observer to estimate the disturbances and use the estimate in the prediction. We choose the second idea and identify the augmented initial state  $\tilde{x}_0$  and the parameters of the current model  $\theta$  as exogenous parameters of the NLP

$$\mathcal{P}_{\text{MPC}}(\tilde{x}_0, \theta) := \underset{w}{\text{minimize}} \quad \Phi(w) \quad (8a)$$

$$\text{subject to} \quad G(w, \tilde{x}_0, \theta) = 0, \quad (8b)$$

$$H(w) \leq 0, \quad (8c)$$

that represents the discrete time OCP (1). Important to note is that the system dynamics are part of (8b) and in standard offset-free MPC, the disturbances are assumed to be constant over the predicted trajectory with  $d_k = \tilde{d}$  for  $k = 0, \dots, N-1$ , where  $\tilde{d}$  denotes the recent disturbance estimate. The feedback control law of the NMPC scheme is given by the solution map  $u_0^* : \mathbb{R}^{n_x} \rightarrow \mathbb{R}^{n_u}$ ,  $\tilde{x}_0 \mapsto u_0^*$  corresponding to the parametric NLP with fixed  $\theta$ . For each evaluation of the solution map, a high-dimensional non-convex NLP has to be solved. We follow standard practice to consider the initial state as a parameter. We also do this for the parameters of the current map to be able to adapt them iteratively in a later section. Although this control scheme is easy to implement, it is only capable of reacting to disturbances after they have influenced the behavior of the ship. Refer to the third plot of Figure 1. In the next section, this controller is extended to exploit previous experience in an ILC scheme.

## IV. EXTENSION TO ITERATIVE LEARNING CONTROL

Ferries and water taxis usually transit on predefined waterways repeatedly under similar operation conditions. To

exploit experiences gained in previous trials of a repeated task, the ILC framework can be employed. For special cases such as perfect tracking, it has been shown that zero-order updates of the model used in an NMPC scheme converge to the optimal solution [15]. In our proposed iterative learning NMPC scheme, we aim to learn the disturbance model along the optimal path iteratively. To model the disturbances, a data-driven approach is chosen based on the dataset

$$\mathbb{D} = \begin{bmatrix} (\hat{s}_0, \hat{d}_0) \\ (\hat{s}_1, \hat{d}_1) \\ \vdots \\ (\hat{s}_{D-1}, \hat{d}_{D-1}) \end{bmatrix},$$

given by  $D$  tuples each containing the estimated traveled distance along the path denoted by  $\hat{s}_{1,k}$  and the corresponding current estimate at this position  $\hat{d}_k$  with  $k = 0, \dots, D-1$ . The tuples are sorted in the database, such that  $\hat{s}_k \leq \hat{s}_{k+1}$  holds for  $k = 0, \dots, D-1$ . Aware that the database could be used in different regression methods to model the disturbances, we use a data-driven approach where the database is used directly  $\theta \equiv \mathbb{D}$ . The advantages of this data-driven approach are that no prior information in the form of a basis function is required and the model's accuracy can be improved by enlarging the number of data tuples. The disadvantage of outliers also having a major influence on the model is not relevant in the investigated application, as the data points are already smoothed by the employed filter algorithm. Removing old data tuples has the advantage of limited memory requirements and the ability to adapt to time varying disturbances. To model the current field a linear interpolation between the two adjacent points given by

$$\hat{\eta}_{c,M}(\eta, \theta) = \frac{\hat{d}_{k+1} - \hat{d}_k}{\hat{s}_{k+1} - \hat{s}_k} (s - \hat{s}_k) + \hat{d}_k$$

is used, where  $s$  denotes the traveled distance along the path and with  $\hat{s}_k \leq s < \hat{s}_{k+1}$ , the traveled distance is located between these data points. In the case of only one neighbor, the current is set to zero. Using the ILC approach, experiences from the last trials are used to get a better

---

#### Algorithm 1 Iterative Learning-Based NMPC

---

**Input:**  $\theta_0, \hat{x}_0$ : Initial parameter guesses;  
 $w_0$ : Initial guess for  $\mathcal{P}_{\text{MPC}}(\hat{x}_0, \theta_0)$ ;  
1: **for**  $i \in \{0, 1, 2, \dots, n_{\text{trial}} - 1\}$  **do**  
2:    $\mathbb{D} \leftarrow \emptyset$ ;  
3:   **for**  $k \in \{0, 1, 2, \dots, n_{\text{process}} - 1\}$  **do**  
4:      $\hat{x}_k \leftarrow \text{GetStateAndDisturbanceEstimate}$ ;  
5:      $\mathbb{D} \leftarrow \mathbb{D} \cup \{\hat{x}_k, \hat{d}_k\}$ ;  
6:      $w^* \leftarrow \text{Solver}(\mathcal{P}_{\text{MPC}}(\hat{x}_k, \theta_i), w_k)$ ;  
7:      $u_k^* \leftarrow \text{SelectFirstControl}(w^*)$ ;  
8:      $\text{SendToActuators}(u_k^*)$ ;  
9:      $w_{k+1} \leftarrow \text{Shift}(w^*)$ ;  
10:   **end for**  
11:    $\theta_{i+1} \leftarrow \text{UpdateModelParameters}(\theta_i, \mathbb{D})$ ;  
12: **end for**

---

prediction for the currents along the trajectory. The iterative procedure to optimize both, the closed-loop performance and the local disturbance model around the optimal trajectory is described in the form of pseudo-code in Algorithm 1. As discussed, the presented setting considers box constraints on the inputs. Therefore, it is reasonable to assume the existence of a solution in step 6. After the disturbance model is converged, a standard NMPC setting is given, which can be analyzed using known methods. Usually, in model-based reinforcement learning approaches global models of the dynamics including disturbances are learned using (deep) neural networks [22]. However, using the considered ILC approach a local but highly accurate data-driven model around the optimal trajectory is identified specifically for the given task. This goes hand in hand with the advantages of being easily interpretable, treatable with efficient solvers, data efficient, and computationally cheap. In the following section, an application example is presented.

## V. EXPERIMENTS

In this section, the described methods are applied to a repeated transit scenario of the research vessel *Solgenia* in simulation. In the following, the experimental setup is specified. Subsequently, the results are shown and discussed.

### A. Setup

In the investigated scenario, the vessel's task is to follow a straight path connecting two waypoints while it is disturbed by an a priori unknown current field. The vessel is driven in the underactuated *transit mode*. Note that this is a typical scenario for autonomous water taxis or autonomous ferries [2], [3]. Without loss of generality, we define the local frame such that the starting waypoint is located at the origin and the second waypoint is located at  $(x_{\text{aim}}, 0)$  with  $x_{\text{aim}} > 0$ . The different parts of the application scenario are specified in the following. The corresponding parameters are listed in Table I and the model of the vessel's dynamics and its parameters, identified with full-scale experiments, is given in [20].

1) *Dynamics and Actuator Configuration*: The research vessel *Solgenia* shown in Figure 2 has two propellers. One bow thruster with a fixed orientation is located in the front of the vessel and a 360°-pivotable main thruster with steering angle  $\alpha$  is located at the rear of the vessel. Thus, the control vector contains  $n_a = 3$  dimensions and is given by  $a = (n_{\text{AT}}, \alpha, n_{\text{BT}})^\top$ . However, in transit mode, the turn rate of the main thruster denoted by  $n_{\text{AT}}$  is fixed and with  $n_{\text{BT}} = 0$  the bow thruster is deactivated. Thus with  $a^- = \alpha$  the steering angle is the only system input in this configuration.

2) *Current Field*: Current fields occurring in real-world scenarios represent solutions of partial differential equations (PDE) that are hard to model. Therefore, current fields are often modeled using empirical data instead of modeling and numerically solving PDEs. As an example, the amplitudes of a linear interpolation model based on full-scale data are depicted in Figure 3. To investigate the presented control algorithms, we use a scenario with a crossing of narrow

TABLE I  
PARAMETERS SPECIFYING THE APPLICATION SCENARIO –  
ALL VALUES ARE GIVEN IN SI UNITS

Par	Value	Par	Value	Par	Value	Par	Value
$N_{\text{sim}}$	3000	$\bar{c}_x$	-0.5	$q$	50	$\Sigma_{\text{init}}$	$\mathbb{I}_{8 \times 8}$
$\Delta T_{\text{sim}}$	0.1	$x_s$	50	$r$	200	$\Sigma_x$	$\mathbb{I}_{8 \times 8}$
$n_x$	6	$x_e$	100	$N$	20	$\Sigma_y$	$\mathbb{I}_{6 \times 6}$
$n_{\bar{x}}$	9	$m_x$	1	$\Delta T_k$	1	$\hat{x}_0$	$0_{8 \times 1}$
$n_y$	6	$\bar{c}_y$	-0.2	$n_{\text{step}}$	10	$K_{p,\psi}$	5.22
$n_u$	3	$y_s$	-10	$n_{\text{AT}}$	10	$K_{d,\psi}$	33.76
$n_u^-$	1	$y_e$	-3	$n_{\text{BT}}$	0	$K_{p,r}$	0.16
$\hat{x}_0$	$0_{6 \times 1}$	$m_y$	1	$D$	300	$K_{d,r}$	7.67

waterways. To model this scenario, the ground truth non-rotational current field with smooth steps between different amplitudes is assumed and given by

$$\dot{\eta}_c(\eta) = \begin{pmatrix} \frac{\bar{c}_x}{\pi} [\arctan(m_x(y_1 - y_s)) - \arctan(m_x(y_1 - y_e))] \\ \frac{\bar{c}_y}{\pi} [\arctan(m_y(x_1 - x_s)) - \arctan(m_y(x_1 - x_e))] \\ 0 \end{pmatrix},$$

where  $\bar{c}_x, \bar{c}_y \in \mathbb{R}$  denote the current magnitudes, and  $m_x, m_y, x_s, x_e, y_s, y_e \in \mathbb{R}$  are further parameters for shaping.

3) *Cost Function*: To follow a desired path with a minimum control effort, the cost function is defined in the form of least squares as

$$l(e(x_k, u_k)) = q y_{1,k}^2 + r \alpha_k^2,$$

where  $q, r > 0$  denote weighting coefficients. Note that due to the chosen local frame the magnitude of  $y_{1,k}$  is equal to the vessel's distance to the reference path at time step  $k$ . Further, the matrix  $P$  used in the terminal cost function (4) is determined as the solution of the *algebraic Riccati equation in discrete time* based on the linearized dynamics [17].

4) *Sensor Fusion Settings*: We assume Gaussian distributions for the process noise  $w_k \sim \mathcal{N}(0, \Sigma_x)$  and the measurement noise  $v_k \sim \mathcal{N}(0, \Sigma_y)$  with zero-mean and covariance matrices  $\Sigma_y, \Sigma_x \succ 0$ . To estimate the state vector and the disturbances, an Extended Kalman Filter (EKF) can be employed. This EKF is initialized with a prior Gaussian distribution  $\hat{x}_0 \sim \mathcal{N}(x_{\text{init}}, \Sigma_{\text{init}})$  with mean  $x_{\text{init}}$  and covariance  $\Sigma_{\text{init}} \succ 0$ . While the estimation of the state and the current using the measurement data is illustrated, ideal state estimation is assumed in the following to be able to clearly evaluate the performance of the different control algorithms.

5) *ILC Settings*: In the investigated experimental setting, after each trial the previous parameters of the current model are replaced by the data recorded in the previous trial. Numerical experiments have shown that this is an appropriate choice. Other settings of the used model and other procedures for updating the parameters are also possible.

6) *Compared Controllers*: To investigate the presented iterative learning-based NMPC algorithm, we compare it to other control approaches suitable to the presented underactuated path following task. These are:

- *Reference*: Disturbance reaction NMPC with a perfect current model as optimal, but not practicable baseline.
- *Method A*: A track controller based on linear subordinated control loops [19].

TABLE II  
QUALITY CRITERIA OF THE INVESTIGATED APPROACHES

	Mean Costs	Max. Error	Max. Steering	Distance
Reference	0.35	0.41 m	20.0°	203.4 m
Method A	5.63	2.35 m	53.1°	186.5 m
Method B	2.60	1.74 m	43.3°	196.4 m
Method C	0.35	0.41 m	20.0°	203.4 m

- *Method B*: Disturbance reaction offset-free NMPC without a current model [17].
- *Method C*: Iterative learning-based NMPC without prior current knowledge (this paper).

To ensure a fair comparison besides the described differences, the identical setting is used for the optimization-based approaches and the gains of the linear track controller are selected to minimize the closed-loop costs corresponding to the scenario. The different control approaches are implemented via the MATLAB interface of CasADi [23] and the NLPs are solved numerically with IPOPT [24].

## B. Results

The resulting trajectories are shown in Figure 1 with a schematic drawing of the vessel's pose including its orientation every 15 s. The corresponding actuator trajectories are shown in Figure 4. All investigated controllers lead to acceptable behavior. In *Method A*, the disturbance reaction is given by a contracting oscillation. After the 5<sup>th</sup> trial the *Reference* and *Method C* show nearly equal behavior. These methods react in a predictive way to the disturbance. Due to a slight steering action, the vessel's heading is turned before the current influences the vessel's dynamics. Therefore, nearly perfect path tracking with a tracking error of less than 0.41 m is possible although the used underactuated setting. In addition, the controller utilizes the current and the associated forces to accelerate the ship in the direction of the path. Employing *Method B* the NMPC scheme can react to the disturbance after it influences the vessel's dynamics. Consequently, the tracking error reaches a maximum amplitude of 1.74 m and a higher effort for the disturbance reaction is required compared to the *Reference* resp. *Method C*. However, due to the disturbance estimation used in *Method B*, the controlled vessel reaches the path although no prior disturbance model is given. To compare the results, the following criteria are defined and evaluated in Table II:

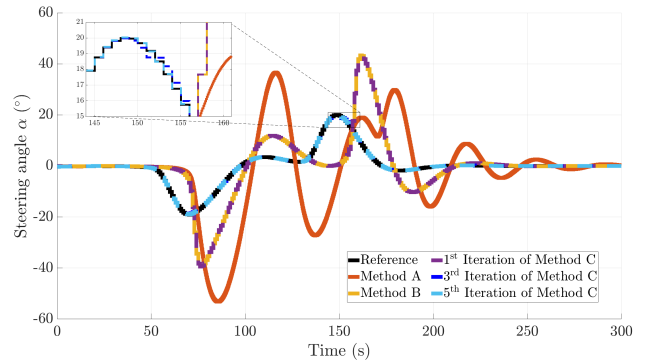


Fig. 4. Actuator trajectories using the different control approaches.

- 1) Mean cost: The mean stage costs over the whole experiment, given by  $\frac{1}{N_{\text{sim}}} \sum_{k=0}^{N_{\text{sim}}} L(x_k, u_k)$ .
- 2) Max. error: The tracking error with the maximum magnitude while processing, given by  $\max_k |y_{1,k}|$ .
- 3) Max. steering: The steering angle with maximum magnitude while processing, given by  $\max_k |\alpha_k|$ .
- 4) Distance: Traveled distance at the end of the simulation experiment, given by  $x_{1,N_{\text{sim}}}$ .

Note that the traveled distance is proportional to the average velocity. The mean cost achieved by *Method C* is decreasing from trial to trial. Starting with 2.6 in the 1<sup>st</sup> trial and in the 5<sup>th</sup> trial 0.35 is reached. The first trial with no model is equal to *Method B* and the last trial is similar to the *Reference*. Interestingly, *Method C* outperforms *Method B* in all criteria while both methods are based on the same OCPs only differing in the type of disturbance model. The experiments show the potential of ILC in combination with NMPC and disturbance observers. The widespread linear track controller is not competitive with the optimization-based approaches.

## VI. CONCLUSION AND FUTURE WORK

This paper presents a learning-based NMPC method for path following control of an underactuated vessel. The key feature of the presented method is the use of disturbance estimates within a simple data-driven disturbance model. The numerical experiments illustrate the possibility of improving the behavior of an ASV by exploiting experiences from previous trials autonomously. The investigation is done using various simulation experiments with a dynamic model of the research vessel *Solgenia*. The presented method could contribute to the design of efficient autonomous maritime transportation systems because a path can be followed with high accuracy even in environments with strong currents. In future work, it would be of interest to investigate the convergence properties of the presented method, to perform full-scale experiments in real current fields, and to investigate the method's real-time capability while employing embedded solvers. Moreover, it would be interesting to extend the setting to also consider interactions between different vessels in inland water scenarios.

## REFERENCES

- [1] J. E. Walmsness, H. H. Helgesen, S. Larsen, G. K. M. Kufalor, and T. A. Johansen, "Automatic dock-to-dock control system for surface vessels using bumpless transfer," *Ocean Engineering*, vol. 268, p. 113425, 2023.
- [2] E. F. Brekke, E. Eide, B.-O. H. Eriksen, E. F. Wilthil, M. Breivik, E. Skjellaug, Ø. K. Helgesen, A. M. Lekkas, A. B. Martinsen, E. H. Thyri, T. Torben, E. Veitch, O. A. Alsos, and T. A. Johansen, "milliampere: An autonomous ferry prototype," *Journal of Physics: Conference Series*, vol. 2311, no. 1, p. 012029, 2022.
- [3] W. Wang, D. Fernández-Gutiérrez, R. Doornbusch, J. Jordan, T. Shan, P. Leoni, N. Hagemann, J. K. Schiphorst, F. Duarte, C. Ratti, and D. Rus, "Roboat iii: An autonomous surface vessel for urban transportation," *Journal of Field Robotics*, vol. 40, no. 8, pp. 1996–2009, 2023.
- [4] Y. Gu and S. W. Wallace, "Operational benefits of autonomous vessels in logistics—a case of autonomous water-taxi in bergen," *Transportation Research Part E: Logistics and Transportation Review*, vol. 154, p. 102456, 2021.

- [5] G. Bitar, M. Breivik, and A. M. Lekkas, "Energy-optimized path planning for autonomous ferries," *IFAC-PapersOnLine*, vol. 51, no. 29, pp. 389–394, 2018.
- [6] M. Lutz and T. Meurer, "Optimal trajectory planning and model predictive control of underactuated marine surface vessels using a flatness-based approach," in *2021 American Control Conference (ACC)*, pp. 4667–4673, IEEE, 2021.
- [7] J. M. Manzano, J. R. Salvador, G. Bejarano, and D. Limon, "Nonlinear model predictive control applied to robust guidance of autonomous surface vehicles," in *2021 60th IEEE Conference on Decision and Control (CDC)*, pp. 5735–5740, IEEE, 2021.
- [8] K. Bergman, O. Ljungqvist, J. Linder, and D. Axehill, "An optimization-based motion planner for autonomous maneuvering of marine vessels in complex environments," in *2020 59th IEEE Conference on Decision and Control (CDC)*, pp. 5283–5290, IEEE, 2020.
- [9] A. B. Martinsen, A. M. Lekkas, and S. Gros, "Autonomous docking using direct optimal control," *IFAC-PapersOnLine*, vol. 52, no. 21, pp. 97–102, 2019.
- [10] L. Streichenberg, E. Trevisan, J. J. Chung, R. Siegwart, and J. Alonso-Mora, "Multi-agent path integral control for interaction-aware motion planning in urban canals," in *2023 IEEE International Conference on Robotics and Automation (ICRA)*, pp. 1379–1385, IEEE, 2023.
- [11] J. R. Marx, R. Damerius, and T. Jeansch, "Linearized model predictive control with offset-freeness for trajectory tracking on inland vessels," in *2023 31st Mediterranean Conference on Control and Automation (MED)*, pp. 692–697, IEEE, 2023.
- [12] A. Doering, M. Wiggert, H. Krasowski, M. Doshi, P. F. Lermusiaux, and C. J. Tomlin, "Stranding risk for underactuated vessels in complex ocean currents: Analysis and controllers," in *2023 62nd IEEE Conference on Decision and Control (CDC)*, pp. 7055–7060, IEEE, 2023.
- [13] D. Kim, T. Tezdogan, and A. Incecik, "A high-fidelity cfd-based model for the prediction of ship manoeuvrability in currents," *Ocean Engineering*, vol. 256, p. 111492, 2022.
- [14] H. Homburger, S. Wirtensohn, M. Diehl, and J. Reuter, "Energy-optimal planning and shrinking horizon mpc for vessel docking in river current fields," in *2024 European Control Conference (ECC)*, pp. 1125–1130, IEEE, 2024.
- [15] K. Baumgartner and M. Diehl, "Zero-order optimization-based iterative learning control," in *2020 59th IEEE Conference on Decision and Control (CDC)*, pp. 3751–3757, IEEE, 2020.
- [16] S. Li, C. Xu, J. Liu, and B. Han, "Data-driven docking control of autonomous double-ended ferries based on iterative learning model predictive control," *Ocean Engineering*, vol. 273, p. 113994, 2023.
- [17] J. B. Rawlings, D. Q. Mayne, and M. M. Diehl, *Model predictive control: Theory, computation, and design*. Madison: Nob Hill Publishing, 2. ed. ed., 2020.
- [18] H. G. Bock and K. J. Plitt, "A multiple shooting algorithm for direct solution of optimal control problems \*," *IFAC Proceedings Volumes*, vol. 17, no. 2, pp. 1603–1608, 1984.
- [19] T. I. Fossen, *Handbook of Marine Craft Hydrodynamics and Motion Control*. Wiley, 2011.
- [20] H. Homburger, S. Wirtensohn, M. Diehl, and J. Reuter, "Feature-based mppi control with applications to maritime systems," *Machines*, vol. 10, no. 10, p. 900, 2022.
- [21] S. Wirtensohn, M. Schuster, and J. Reuter, "Disturbance estimation and wave filtering using an unscented kalman filter," *IFAC-PapersOnLine*, vol. 49, no. 23, pp. 518–523, 2016.
- [22] V. François-Lavet, P. Henderson, R. Islam, M. G. Bellemare, and J. Pineau, "An introduction to deep reinforcement learning," *Foundations and Trends® in Machine Learning*, vol. 11, no. 3-4, pp. 219–354, 2018.
- [23] J. A. E. Andersson, J. Gillis, G. Horn, J. B. Rawlings, and M. Diehl, "Casadi: a software framework for nonlinear optimization and optimal control," *Mathematical Programming Computation*, vol. 11, no. 1, pp. 1–36, 2019.
- [24] A. Wächter and L. T. Biegler, "On the implementation of an interior-point filter line-search algorithm for large-scale nonlinear programming," *Mathematical Programming*, vol. 106, no. 1, pp. 25–57, 2006.